

# The Effect of Dynamic Structural Flexibility in Halide Perovskites

Christian Gehrman<sup>+</sup>, Sebastián Caicedo-Dávila<sup>+</sup>, Xiangzhou Zhu,  
and David A. Egger<sup>\*</sup>

Department of Physics, Technical University of Munich, Garching, Germany

## Abstract

Despite their puzzling vibrational characteristics that include strong signatures of anharmonicity and thermal disorder already around room temperature, halide perovskites exhibit favorable optoelectronic properties for applications in photovoltaics and beyond. Whether these vibrational properties are advantageous or detrimental to their optoelectronic properties remains, however, an important open question. Here, this issue is addressed by investigation of the origin and consequences of the dynamic structural flexibility in the prototypical cubic  $\text{CsPbBr}_3$ , using first-principles molecular dynamics based on density-functional theory. It is shown that the dynamic flexibility associated with halide perovskites enables the so-called *transversality*, which manifests as a preference for large halide displacements perpendicular to the Pb-Br-Pb bonding axis. We find that transversality is concurrent with vibrational anharmonicity and short-ranged disorder correlations, which is favorable for photovoltaics since it implies sharp optical absorption profiles. These findings are contrasted to the case of PbTe, a material that shares several key properties with  $\text{CsPbBr}_3$  but cannot exhibit any transversality and, hence, is found to exhibit much wider band-edge distributions. We conclude that the dynamic structural flexibility in halide perovskites as well as their unusual vibrational characteristics might not just be a mere coincidence, but could play active roles in establishing their favorable optoelectronic properties.

---

<sup>+</sup>These authors contributed equally

<sup>\*</sup>Email Address: david.egger@tum.de

Halide perovskites (HaPs) are semiconducting materials with an enormous potential for various technological applications, perhaps most notably for photovoltaics.[1–4] Significant interests in these systems are motivated by their favorable optoelectronic properties and the simultaneous availability of low-cost synthesis and fabrication routes.[5–8] Among their many outstanding physical and chemical characteristics, the structural dynamical properties of HaPs are especially intriguing.[9–11] In particular, significant vibrational anharmonicities have been detected in these and related systems already at room temperature.[12–21] The unusual lattice vibrational properties of HaPs have already been shown to influence some key optoelectronic quantities including the band-gap energy,[22] charge-carrier mobilities, [23–25] defect energetics, [26–31] the Urbach energy, [32, 33] carrier recombination rates and ion migration barriers,[34–37] Whether the peculiar lattice vibrational properties of HaPs are advantageous or detrimental to their optoelectronic properties remains, however, an open question.[37] Since vibrational anharmonicities are known to occur in other optoelectronic materials,[38–47] addressing this question is important because it will support the design of alternative material systems with similarly favorable or improved optoelectronic properties.

In this work, we perform first-principles molecular dynamics (MD) simulations to investigate the origins and consequences of the unusual lattice vibrational properties of HaPs. In characterizing the vibrational features of the prototypical cubic CsPbBr<sub>3</sub> we highlight a distinctive property – which we call *transversality* – that showcases the high degree of *dynamic structural flexibility in HaPs*. Transversality is shown to derive naturally from the octahedral arrangement of halide ions in the perovskite lattice and to coincide with large vibrational displacements and anharmonicities in the system. Importantly, the dynamic structural flexibility of HaPs as expressed in transversality is found to have a strong effect on disorder correlations that are important for optoelectronic properties including finite-temperature band-gap energy distributions. We contrast the findings for CsPbBr<sub>3</sub> to the case of PbTe, which shares several important characteristics with prototypical HaPs but, due to its rocksalt structure, cannot exhibit any transversality, in order to demonstrate that absence of this feature is detrimental to optoelectronic properties. Our results suggests that the peculiar lattice vibrational properties of HaPs might not just be a mere coincidence, but rather could potentially play an active role in determining the favorable optoelectronic properties of these materials.

We consider the prototypical HaP material CsPbBr<sub>3</sub>, which is known to exhibit, on average, a cubic-symmetry structure of corner-sharing octahedra and void-filling A-site cations at temperatures above  $\sim 400$  K.[48–50] Performing MD calculations based on density functional theory (DFT) at a temperature of 425 K (see Methods section), allows for depicting the finite-temperature, real-time structure of cubic CsPbBr<sub>3</sub>, including a description of the appearing vibrational anharmonicity to all orders. Our goal here is to investigate how specific patterns in the vibrational features of the system impact optoelectronic properties. Since electronic states close to the band edges of HaPs in general, and CsPbBr<sub>3</sub> in particular, are formed by the lead and halide atomic orbitals, we focus on the Pb-Br-Pb network and motions of halides therein, and stipulate to describe the finite-temperature Br displacements by two directional components: either Br moves along the Pb-Br-Pb bond axis (blue line in **Figure 1a**) or it moves on a 2D plane that is perpendicular to that axis (light-orange plane in Figure 1a). Thus, any Br displacement occurring at finite temperature is characterized by its *longitudinal* (along the Pb-Br-Pb bond axis) and *transversal* components (perpendicular to the Pb-Br-Pb bond axis).

For each structure occurring along the MD trajectory we hence define a transversality,  $\eta$ , as follows

$$\eta = \frac{1}{N_{\text{Br}}} \sum_{i=1}^{N_{\text{Br}}} \frac{d_i^{\text{transv}}}{d_i^{\text{longi}}} , \quad (1)$$

where  $N_{\text{Br}}$  is the number of Br atoms in the supercell and  $d_i^{\text{transv/longi}}$  are the norms of the

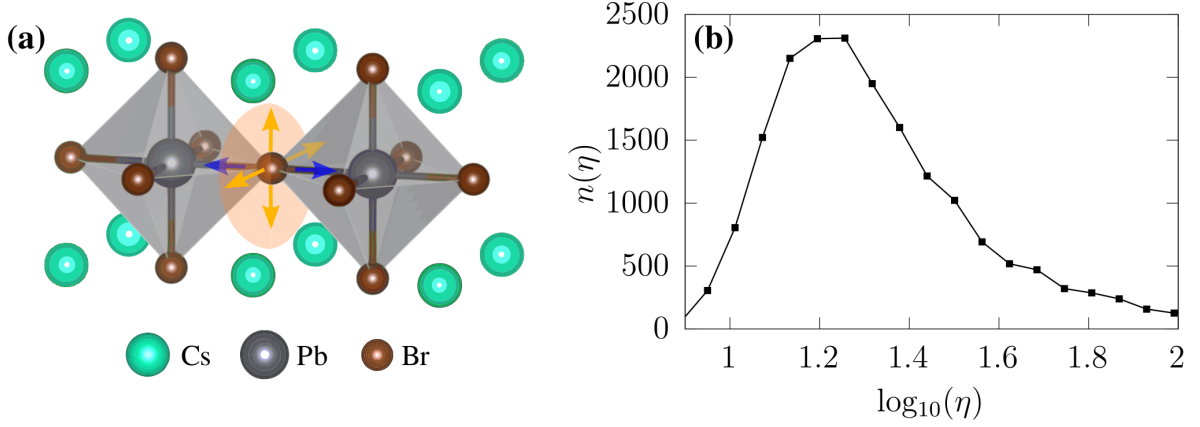


Figure 1: **(a)** Schematic structural representation of cubic  $\text{CsPbBr}_3$  and the displacements of Br ions at finite-temperature: longitudinal components occur in parallel to the Pb-Br-Pb bonding axis (blue arrows) and transversal components perpendicular to it (yellow arrows expanding the light-orange plane). **(b)** Histogram of transversality,  $\eta$ , as defined in Eq. 1, calculated along the MD trajectory at 425 K. Note that this is shown as a semi-log plot.

transversal / longitudinal displacement components of the  $i$ th Br ion. We present additional means of comparing the occurrence of transversal and longitudinal displacements in the Supporting Information (SI). Calculating the histogram of  $\eta$  along the MD trajectory (see Figure 1b) reveals that  $\text{CsPbBr}_3$  in its cubic structure features large transversal Br displacements: the histogram peaks at  $\eta \approx 20$ , with a significant tail at high values of  $\eta$ , up to  $\eta \approx 100$ , and quickly decreases to zero when approaching  $\eta = 1$ . This indicates that the movements of Br ions are very much favored on the 2D-planes perpendicular to Pb-Br-Pb bond axis compared to movements along it, which suggests a peculiar directionality in the finite-temperature dynamics of  $\text{CsPbBr}_3$  despite the fact that, on average, it exhibits a cubic symmetry. Interestingly, the appearance of transversality is closely connected to the rotations of the  $\text{PbBr}_6$  octahedra (see SI), which are a known generic feature of the finite-temperature dynamics of HaPs.[51–54] In the SI, we also show that the transversal Br displacements are concurrent with lattice-vibrational anharmonicity in  $\text{CsPbBr}_3$ . The large degree of transversality in the Br ion dynamics signifies an enormous dynamic structural flexibility of HaPs because ions that participate in covalent bonding with Pb are actually favorably displaced *away from the bonding axis*. The occurrence of this property motivates an investigation into its origin and implications for other important characteristics of  $\text{CsPbBr}_3$ . To this end, we analyze the disorder potential generated by the finite-temperature ion dynamics. Specifically, we compute the autocorrelation function of the disorder potential,  $C(\Delta y)$  (see Methods section), for which we have previously found that it is dynamically shortened and approaches a value of zero on length scales on the order of one Pb-X bond.[33] **Figure 2a** shows  $C(\Delta y)$  separately for the longitudinal and transversal components of Br displacements in  $\text{CsPbBr}_3$  at 425 K (see Methods section), in addition to the result from a full MD calculation. While the longitudinal components alone would lead to a long-ranged response, clearly the transversal Br displacements are responsible for the short-ranged nature of the disorder potential in  $\text{CsPbBr}_3$  at finite temperature. Such a short-ranged disorder potential is known to be concurrent with narrower band-edge distributions that imply small values for the Urbach energy,[33, 55] suggesting that the transversality in the Br dynamics is important for the electronic-structure properties.

The reason for the transversality in Br displacements and the short-ranged nature of the disorder potential can be found in the very peculiar way the HaP system responds to changes in its atomic configurations. To illustrate this, we calculated the charge-density response to specific

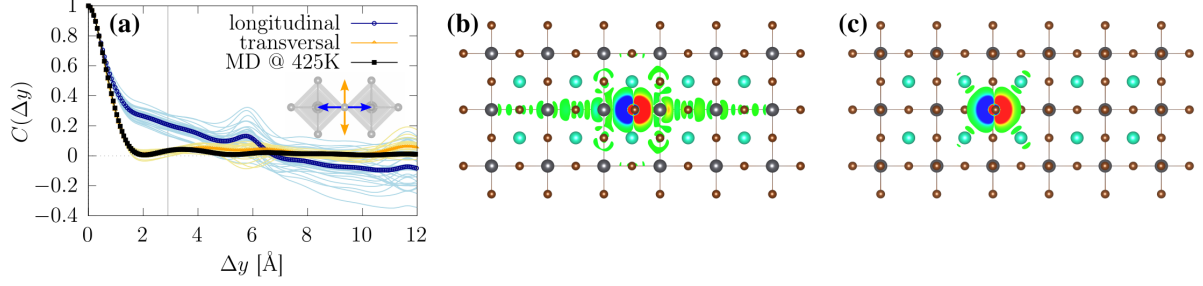


Figure 2: **(a)** Autocorrelation function of the disorder potential,  $C(\Delta y)$ , that is induced by the Br motions along longitudinal (blue) and transversal (yellow) directions in CsPbBr<sub>3</sub> at 425 K. The thin lines correspond to individual snapshots,  $C_i(\Delta y)$  in Eq. (2), and the thick-dotted lines to their average.  $C(\Delta y)$  according to the full set of displacements occurring in the 425 K trajectory is also shown (black line). The inset shows two adjacent PbBr<sub>6</sub> octahedra and depicts the Br displacement directions, and the vertical gray line indicates the nominal Pb-Br bonding distance. Isosurface representation of the calculated charge-density response to a Br displacement along **(b)** longitudinal direction and **(c)** transversal direction in a supercell of CsPbBr<sub>3</sub>. Isosurfaces are shown for changes above  $8.1 \times 10^{-3} e\text{\AA}^{-3}$  ( $e$  being the electron charge).

atomic displacements in an otherwise static supercell of CsPbBr<sub>3</sub> using DFT (see Methods section for details). Displacing a Br ion longitudinally leads to a response in the charge density that is clearly *long-ranged* and spans several unit cells (Figure 2b). In sharp contrast to this scenario, displacing a Br ion transversely leads to a response in the charge density that is clearly *short-ranged* and essentially confined to a single unit cell (Figure 2c). This qualitative difference in the charge-density response comparing transversal and longitudinal Br displacements is related to the resonant bonding mechanism[56, 57] that has been extensively discussed in the literature on HaPs[19, 33, 58] and other materials:[59–62] along the Pb-Br-Pb bond axes, Br-4p<sub>x</sub> and Pb-6s  $\sigma$ -interactions give rise to the valence band and a network of resonant bonds.[63, 64] Displacing an atom along the direction of orbital hybridization leads to changes in the charge density that “resonate” throughout the network: when the symmetry of the network is broken by such a displacement, degeneracies of orbital configurations are lifted, the orbital occupations thus modulated, and a long-ranged response in the charge density must follow (*cf.* Figure 2b). In contrast, any transversal displacement cannot influence the resonant bonding network, since by its definition the transversal plane is orthogonal to the direction of the network, as are the Br-p<sub>y</sub> and Br-p<sub>z</sub> states which do not participate in the resonant bonding. Therefore, the transversal Br displacements essentially do not perturb the resonant network and, hence, only lead to short-ranged changes in the charge density (*cf.* Figure 2c). It is for this reason that transversal Br displacements are highly favored energetically (see SI) over the longitudinal ones and, hence, occur with a much larger likelihood.

Our findings suggest that the dynamic structural flexibility of HaPs, such as CsPbBr<sub>3</sub> with its apparent degree of transversality, may play an active role in determining the favorable optoelectronic properties of HaPs, because a short-ranged disorder potential implies sharper optical absorption onsets. To test this hypothesis, we consider PbTe as a counter-example for a material sharing many key properties with CsPbBr<sub>3</sub> (see SI for detailed discussion): bonding properties including the anti-bonding nature of the VBM formed by  $\sigma$  interactions of anion p and cation s orbitals, the cross-gap hybridization of the anion p orbitals, a stereochemically active lone pair of electrons[65–67] as well as vibrational anharmonicities[38, 39] and, interestingly, a similar type of resonant bonding mechanism[61]. Importantly, however, given its rocksalt structure (see inset in **Figure 3a**), from symmetry considerations PbTe cannot exhibit any degree

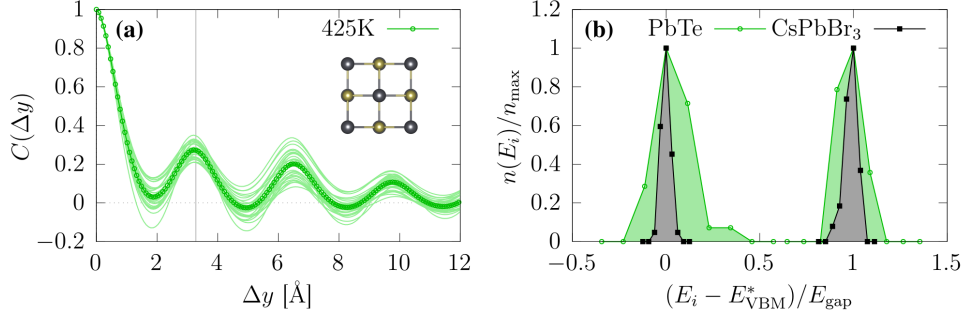


Figure 3: **(a)**  $C(\Delta y)$  for PbTe material calculated at 425 K; the inset depicts a structural representation of this system and the gray vertical line indicates the nominal Pb-Te bonding distance. Panel **(b)** shows normalized histograms of the band-edge energies calculated along the MD trajectories of CsPbBr<sub>3</sub> (black curve) and PbTe (green curve) at 425 K. The histograms were centered to the VBM/CBM energy with highest occurrence,  $E_{\text{VBM/CBM}}^*$ , in order to allow for a direct comparison of the band-edge distributions of CsPbBr<sub>3</sub> and PbTe (see Methods section).

of transversality. As a consequence of the absence of transversality, any atomic displacement must perturb the resonant network to a certain degree, which leads to longer-ranged changes in the charge-density response to atomic displacements, as we explicitly show in the SI. In full agreement with the expectations borne from this reasoning, we find features in  $C(\Delta y)$  for PbTe (see Figure 3a) reaching beyond several unit cells when we perform MD at 425 K, which is in sharp contrast to the ultra short-ranged correlations found in CsPbBr<sub>3</sub> (*cf.* Figure 2a); note that the oscillatory features can be explained by thermal noise that is due to the atomic displacements modulating the crystal periodic potential (see SI). Most importantly, comparing the conduction and valence band histograms of PbTe and CsPbBr<sub>3</sub> (see Figure 3b) shows that the absence of transversality leads to much broader distributions, which implies a larger amount of thermally-induced tail-states and energetic disorder and, thus, less sharp optical absorption edges and larger Urbach energies. We therefore speculate that the much larger Urbach energy of PbTe[68] compared to CsPbBr<sub>3</sub>[69] could in part be due to its more long-ranged disorder correlations that we have demonstrated here to be a direct consequence of the absence of transversality, keeping in mind that other extrinsic factors may impact the Urbach energy of HaPs too.[70] Altogether, these findings demonstrate that the dynamic structural flexibility of CsPbBr<sub>3</sub> that we characterized here by the large degree of transversality in the Br displacements, potentially plays an important role in establishing the favorable optoelectronic properties of HaPs.

Finally, we would like to put our work in context of recent findings in the literature. Several recent studies reported an important role of specific vibrational modes that are very similar or at least closely related to the transversal modes we highlight here: *e.g.*, the two-dimensional overdamped fluctuations recently found in CsPbBr<sub>3</sub>[22] as well as the X-Pb-X scissoring mode.[71], both of which have also been discussed to imply certain dynamic modulations to the band gap.[22, 71] Another case in point that these modes are relevant for the optoelectronic properties of HaPs is that their counterparts, *i.e.*, the longitudinal modes, were previously found to be involved in so-called cage vibrations that were discussed to be the main finite-temperature contributors to the Urbach energy.[72] This assessment is in full agreement with the expectations borne from our findings that disorder correlations associated with longitudinal displacements would be longer ranged (*cf.* Figure 2). Therefore, we believe that our findings motivate a wider investigation of how the dynamic structural flexibility in HaPs and related materials could be exploited towards design of materials with improved properties.

In summary, we investigated the origin and consequences of dynamic structural flexibility in HaPs by means of first-principles MD for the prototypical model system CsPbBr<sub>3</sub> in the cubic phase. We found that the vibrations in the HaP lattice feature a distinctive property of transversality, which describes the large displacements of halide ions along directions that are orthogonal to the Pb-Br-Pb bonding axis. It was demonstrated that this property leads to a shortening of disorder correlations, which implies a sharpening of the distribution of band edges, a reduction of the number of thermally induced tail-states and, by extension, lowering the Urbach energy. We have also contrasted these findings to the case of PbTe, a similarly anharmonic material also exhibiting resonant bonding and a similar electronic structure, but lacking the dynamic structural flexibility of the perovskite lattice as expressed in transversality. Our findings establish the important link between dynamic structural flexibility of HaPs with their favorable optoelectronic properties. This suggests that the unusual lattice vibrational properties of HaPs might not just be a mere coincidence and could be used to guide the material design of new compounds with similarly favorable or even enhanced optoelectronic properties.

## Methods

### Static DFT Calculations

DFT calculations were performed with the Vienna Ab-initio Simulation Package (VASP) code,[73] using the projector-augmented wave (PAW) method[74] applying the "normal" version of the code-supplied PAW potentials unless otherwise noted. Exchange-correlation interactions were described using the Perdew-Burke-Ernzerhof (PBE) form of the generalized gradient approximation,[75] including corrections for dispersive interactions according to the Tkatchenko-Scheffler scheme.[76] This setup has been shown to allow for an accurate description of the finite-temperature structural dynamics of HaPs.[77] The ionic and lattice degrees-of-freedom of CsPbBr<sub>3</sub> were optimized, starting from a cubic structure, resulting in a final lattice constant of 5.81 Å. For PbTe, we used a conventional rocksalt unit cell (8 atoms), obtained from the Crystallography Open Database,[78] (COD-ID: 9008696)[79] and relaxed it to a lattice constant of 6.56 Å. For structural relaxation and static DFT calculations, an energy convergence threshold of  $10^{-8}$  eV, a  $\Gamma$ -centered  $k$ -grid of  $6 \times 6 \times 6$  and a plane-wave cutoff energy of 500 eV (CsPbBr<sub>3</sub>) and 375 eV (PbTe) were used. The geometries of CsPbBr<sub>3</sub> and PbTe were optimized until residual forces were below  $10^{-3}$  eVÅ<sup>-1</sup>.

### First-Principles MD Calculations

DFT-MD simulations were performed on a  $4 \times 4 \times 2$  (160 atoms) supercell of CsPbBr<sub>3</sub> and a  $3 \times 3 \times 2$  (144 atoms) of PbTe, using the canonical ( $NVT$ ) ensemble at  $T = 425$  K with a Nosé-Hoover thermostat as implemented in the VASP code.[80] The simulation timestep was set to 8 fs for CsPbBr<sub>3</sub> and 10 fs for PbTe. For the sake of efficiency, different settings for the self-consistent calculations in each ionic step were employed: the "GW" PAW potentials were used, together with plane-wave cutoffs of 250 eV (CsPbBr<sub>3</sub>) and 240 eV (PbTe), a single  $k$ -point and an energy convergence threshold of  $10^{-6}$  eV. The system was equilibrated for 5 ps and a subsequent trajectory of 150 ps was used for analysis.

### Disorder Potentials and Band-Edge Histograms

The disorder potential and band-edge histograms were calculated from snapshots of instantaneous nuclear configurations along the MD trajectory. The electronic structure and electrostatic potentials were then computed using a  $1 \times 1 \times 2$   $k$ -grid for CsPbBr<sub>3</sub> and  $2 \times 2 \times 3$   $k$ -grid for PbTe, preserving the density of  $k$ -points in the supercell as compared with the unit-cell calculations.

The autocorrelation,  $C(\Delta y)$ , was calculated — as detailed in our previous work — as the average of the instantaneous autocorrelations:[33]

$$C_i(\Delta y) = \frac{\langle \Delta V_i(y + \Delta y) \cdot \Delta V_i(y) \rangle}{\langle \Delta V_i(y) \cdot \Delta V_i(y) \rangle} \quad (2)$$

where  $\Delta V_i$  is the  $xz$ -averaged change in the electrostatic potential of configuration  $i$  with respect to the average potential along the trajectory, and  $C(\Delta y)$  is averaged over  $N = 30$  instantaneous configurations. To separate the effect of longitudinal and transversal Br displacements in the calculations of  $C(\Delta y)$ , we modified the MD trajectory as follows: for each Br, we separated the  $x$ ,  $y$  and  $z$  cartesian components of a given displacement into longitudinal and transversal contributions (*cf.* Figure 1a), setting either one of them as well as Cs and Pb displacements to zero. The CBM and VBM distributions in Figure 3b were calculated using the respective eigenvalues obtained from DFT calculations performed for 90 configurations along the MD trajectory. These histograms were centered to the VBM/CBM energy with highest occurrence,  $E_{\text{VBM/CBM}}^*$ , using  $E_{\text{gap}}^* = E_{\text{CBM}}^* - E_{\text{VBM}}^*$  normalizing to the respective count, that is  $n_{\text{max}} = n(E_{\text{VBM/CBM}}^*)$ . The normalization allows for a direct comparison of the band-edge distributions of CsPbBr<sub>3</sub> and PbTe despite their different values of the band gap.

## Acknowledgements

The authors thank Laura Herz (University of Oxford) and Omer Yaffe (Weizmann Institute of Science) for fruitful discussions. Funding provided by the Alexander von Humboldt-Foundation in the framework of the Sofja Kovalevskaja Award, endowed by the German Federal Ministry of Education and Research, by the Deutsche Forschungsgemeinschaft (DFG, German Research Foundation) via SPP2196 Priority Program (CH 1672/3-1) and via Germany’s Excellence Strategy - EXC 2089/1-390776260, and by the Technical University of Munich - Institute for Advanced Study, funded by the German Excellence Initiative and the European Union Seventh Framework Programme under Grant Agreement No. 291763, are gratefully acknowledged. The authors further acknowledge the Gauss Centre for Supercomputing e.V. for funding this project by providing computing time through the John von Neumann Institute for Computing on the GCS Supercomputer JUWELS at Jülich Supercomputing Centre.

## References

1. H. J. Snaith, *J. Phys. Chem. Lett.* **4**, 3623–3630, DOI 10.1021/jz4020162 (2013).
2. M. A. Green, A. Ho-Baillie, H. J. Snaith, *Nat. Photonics* **8**, 506–514, DOI 10.1038/nphoton.2014.134 (2014).
3. S. D. Stranks, H. J. Snaith, *Nat. Nanotechnol.* **10**, 391–402, DOI 10.1038/nnano.2015.90 (2015).
4. J.-P. Correa-Baena *et al.*, *Science (80-. )*. **358**, 739–744, DOI 10.1126/science.aam6323 (2017).
5. T. M. Brenner *et al.*, *Nat. Rev. Mater.* **1**, 15007, DOI 10.1038/natrevmats.2015.7 (2016).
6. C. C. Stoumpos, M. G. Kanatzidis, *Adv. Mater.* **28**, 5778–5793, DOI 10.1002/adma.201600265 (2016).
7. W. Li *et al.*, *Nat. Rev. Mater.* **2**, DOI 10.1038/natrevmats.2016.99 (2017).
8. P. K. Nayak *et al.*, *Nat. Rev. Mater.* **4**, 269–285, DOI 10.1038/s41578-019-0097-0 (2019).
9. J. M. Frost, A. Walsh, *Acc. Chem. Res.* **49**, 528–535, DOI 10.1021/acs.accounts.5b00431 (2016).

10. D. A. Egger, A. M. Rappe, L. Kronik, *Acc. Chem. Res.* **49**, 573–581, DOI 10.1021/acs.accounts.5b00540 (2016).
11. D. A. Egger *et al.*, *Adv. Mater.* **30**, 1800691, DOI 10.1002/adma.201800691 (2018).
12. L. D. Whalley *et al.*, *Phys. Rev. B* **94**, 1–5, DOI 10.1103/PhysRevB.94.220301 (2016).
13. A. N. Beecher *et al.*, *ACS Energy Lett.* **1**, 880–887, DOI 10.1021/acsenergylett.6b00381 (2016).
14. O. Yaffe *et al.*, *Phys. Rev. Lett.* **118**, 1–6, DOI 10.1103/PhysRevLett.118.136001 (2017).
15. M. A. Carignano *et al.*, *J. Phys. Chem. C* **121**, 20729–20738, DOI 10.1021/acs.jpcc.7b08220 (2017).
16. A. Marronnier *et al.*, *J. Phys. Chem. Lett.* **8**, 2659–2665, DOI 10.1021/acs.jpclett.7b00807 (2017).
17. A. Gold-Parker *et al.*, *Proc. Natl. Acad. Sci. U. S. A.* **115**, 11905–11910, DOI 10.1073/pnas.1812227115 (2018).
18. A. Marronnier *et al.*, *ACS Nano* **12**, 3477–3486, DOI 10.1021/acsnano.8b00267 (2018).
19. T. Zhu, E. Ertekin, *Energy Environ. Sci.* **12**, 216–229, DOI 10.1039/c8ee02820f (2019).
20. R. Sharma *et al.*, *Phys. Rev. Mater.* **4**, 1–6, DOI 10.1103/PhysRevMaterials.4.092401 (2020).
21. J. Klarbring *et al.*, *Phys. Rev. Lett.* **125**, 45701, DOI 10.1103/PhysRevLett.125.045701 (2020).
22. T. Lanigan-Atkins *et al.*, *Nat. Mater.* **20**, 977–983, DOI 10.1038/s41563-021-00947-y (2021).
23. M. Z. Mayers *et al.*, *Nano Lett.* **18**, 8041–8046, DOI 10.1021/acs.nanolett.8b04276 (2018).
24. A. Lacroix *et al.*, *Phys. Rev. Lett.* **124**, 1–6, DOI 10.1103/PhysRevLett.124.196601 (2020).
25. M. J. Schilcher *et al.*, *ACS Energy Lett.* **6**, 2162–2173, DOI 10.1021/acsenergylett.1c00506 (2021).
26. A. V. Cohen *et al.*, *J. Phys. Chem. Lett.* **10**, 4490–4498, DOI 10.1021/acs.jpclett.9b01855 (2019).
27. Y. Wang *et al.*, *J. Phys. Chem. Lett.* **10**, 1617–1623, DOI 10.1021/acs.jpclett.9b00763 (2019).
28. W. Li *et al.*, *J. Phys. Chem. Lett.* **10**, 6219–6226, DOI 10.1021/acs.jpclett.9b02553 (2019).
29. S. Kumar, G. Hodes, D. Cahen, *MRS Bull.* **45**, 478–484, DOI 10.1557/mrs.2020.146 (2020).
30. X. Zhang, M. E. Turiansky, C. G. Van de Walle, *J. Phys. Chem. C* **124**, 6022–6027, DOI 10.1021/acs.jpcc.0c01324 (2020).
31. W. Chu *et al.*, *Angew. Chemie - Int. Ed.* **59**, 6435–6441, DOI 10.1002/anie.201915702 (2020).
32. B. Wu *et al.*, *Nat. Commun.* **10**, 1–10, DOI 10.1038/s41467-019-08326-7 (2019).
33. C. Gehrman, D. A. Egger, *Nat. Commun.* **10**, DOI 10.1038/s41467-019-11087-y (2019).



34. C. G. Bischak *et al.*, *Nano Lett.* **17**, 1028–1033, DOI 10.1021/acs.nanolett.6b04453 (2017).
35. T. Kirchartz *et al.*, *J. Phys. Chem. Lett.* **9**, 939–946, DOI 10.1021/acs.jpcllett.7b03414 (2018).
36. K. T. Munson *et al.*, *Chem* **4**, 2826–2843, DOI 10.1016/j.chempr.2018.09.001 (2018).
37. K. T. Munson, J. R. Swartzfager, J. B. Asbury, *ACS Energy Lett.* **4**, 1888–1897, DOI 10.1021/acsenergylett.9b01073 (2019).
38. O. Delaire *et al.*, *Nat. Mater.* **10**, 614–619, DOI 10.1038/nmat3035 (2011).
39. C. W. Li *et al.*, *Phys. Rev. B* **90**, 1–10, DOI 10.1103/PhysRevB.90.214303 (2014).
40. C. W. Li *et al.*, *Phys. Rev. Lett.* **112**, 1–5, DOI 10.1103/PhysRevLett.112.175501 (2014).
41. A. Lunghi *et al.*, *Nat. Commun.* **8**, DOI 10.1038/ncomms14620 (2017).
42. K. L. Svane, J. K. Bristow, A. Walsh, *J. Phys. Chem. C* **121**, 22010–22014, DOI 10.1021/acs.jpcc.7b04757 (2017).
43. V. Kapil *et al.*, *J. Chem. Theory Comput.* **15**, 3237–3249, DOI 10.1021/acs.jctc.8b01297 (2019).
44. A. M. Sanni, S. N. Lavan, A. S. Rury, *J. Phys. Chem. C* **124**, 13942–13955, DOI 10.1021/acs.jpcc.0c04573 (2020).
45. M. Asher *et al.*, *Adv. Mater.* **32**, DOI 10.1002/adma.201908028 (2020).
46. T. M. Brenner *et al.*, *Phys. Rev. Mater.* **4**, 115402, DOI 10.1103/PhysRevMaterials.4.115402 (2020).
47. M. Menahem *et al.*, *ACS Nano* **15**, 10153–10162, DOI 10.1021/acsnano.1c02022 (2021).
48. H. Shunsuke *et al.*, *J. Phys. Soc. Japan* **37**, 1393–1398, DOI 10.1143/JPSJ.37.1393 (1974).
49. M. Rodová, J. Brožek, K. Nitsch, *J. Therm. Anal.* **71**, 667–673, DOI 10.1023/A:1022836800820 (2003).
50. C. C. Stoumpos *et al.*, *Cryst. Growth Des.* **13**, 2722–2727, DOI dx.doi.org/10.1021/cg400645t (2013).
51. E. H. Smith, N. A. Benedek, C. J. Fennie, *Inorg. Chem.* **54**, 8536–8543, DOI 10.1021/acs.inorgchem.5b01213 (2015).
52. J. Young, J. M. Rondinelli, *J. Phys. Chem. Lett.* **7**, 918–922, DOI 10.1021/acs.jpcllett.6b00094 (2016).
53. D. Ghosh *et al.*, *ACS Energy Lett.* **2**, 2424–2429, DOI 10.1021/acsenergylett.7b00729 (2017).
54. J. Klarbring, *Phys. Rev. B* **99**, 1–7, DOI 10.1103/PhysRevB.99.104105 (2019).
55. C. W. Greeff, H. R. Glyde, *Phys. Rev. B* **51**, 1778–1783, DOI 10.1103/PhysRevB.51.1778 (1995).
56. H. Krebs, *Z. Anorg. Chem.* **278**, 82 (1955).
57. H. Krebs, *Acta Crystallogr.* **9**, 95–108, DOI 10.1107/s0365110x56000255 (1956).
58. D. Weber, *Z. Naturforsch., B* **33**, 1443–1445 (1978).
59. G. Lucovsky, R. M. White, *Phys. Rev. B* **8**, 660–667, DOI 10.1103/PhysRevB.8.660 (1973).
60. K. Shportko *et al.*, *Nat. Mater.* **7**, 653–658, DOI 10.1038/nmat2226 (2008).

61. S. Lee *et al.*, *Nat. Commun.* **5**, 1–8, DOI 10.1038/ncomms4525 (2014).
62. S. Y. Yue, T. Xu, B. Liao, *Mater. Today Phys.* **7**, 89–95, DOI 10.1016/j.mtphys.2018.11.005 (2018).
63. J. Kim *et al.*, *J. Phys. Chem. C* **119**, 4627–4634, DOI 10.1021/jp5126365 (2015).
64. M. G. Goesten, R. Hoffmann, *J. Am. Chem. Soc.* **140**, 12996–13010, DOI 10.1021/jacs.8b08038 (2018).
65. S. H. Wei, A. Zunger, *Phys. Rev. B* **55**, 13605–13610, DOI 10.1103/PhysRevB.55.13605 (1997).
66. U. V. Waghmare *et al.*, *Phys. Rev. B* **67**, 10, DOI 10.1103/PhysRevB.67.125111 (2003).
67. M. K. Brod, M. Y. Toriyama, G. J. Snyder, *Chem. Mater.* **32**, 9771–9779, DOI 10.1021/acs.chemmater.0c03740 (2020).
68. J. Wang *et al.*, *J. Appl. Phys.* **104**, 1–5, DOI 10.1063/1.2970163 (2008).
69. Y. Rakita *et al.*, *Cryst. Growth Des.* **16**, 5717–5725, DOI 10.1021/acs.cgd.6b00764 (2016).
70. K. J. Savill, A. M. Ulatowski, L. M. Herz, *ACS Energy Lett.* **6**, 2413–2426, DOI 10.1021/acsenergylett.1c00776 (2021).
71. T. A. Bird *et al.*, 1–9 (2021).
72. M. Ledinsky *et al.*, *J. Phys. Chem. Lett.* **10**, 1368–1373, DOI 10.1021/acs.jpclett.9b00138 (2019).
73. G. Kresse, J. Furthmüller, *Phys. Rev. B* **54**, 11169–11186, DOI 10.1103/PhysRevB.54.11169 (1996).
74. G. Kresse, D. Joubert, *Phys. Rev. B* **59**, 1758–1775, DOI 10.1103/PhysRevB.59.1758 (1999).
75. J. P. Perdew, K. Burke, M. Ernzerhof, *Phys. Rev. Lett.* **77**, 3865–3868, DOI 10.1103/PhysRevLett.77.3865 (1996).
76. A. Tkatchenko, M. Scheffler, *Phys. Rev. Lett.* **102**, 6–9, DOI 10.1103/PhysRevLett.102.073005 (2009).
77. H. Beck, C. Gehrman, D. A. Egger, *APL Mater.* **7**, DOI 10.1063/1.5086541 (2019).
78. S. Graulis *et al.*, *J. Appl. Crystallogr.* **42**, 726–729, DOI 10.1107/S0021889809016690 (2009).
79. R. W. G. Wyckoff, *The elements and compounds RX and RX<sub>2</sub>* (Interscience Publishers, New York, New York, ed. 2, 1963), vol. 1, pp. 85–237.
80. G. Kresse, J. Hafner, *Phys. Rev. B* **49**, 14251–14269, DOI 10.1103/PhysRevB.49.14251 (1994).